Tetravalent Chromium (Cr^{4+}) as Laser-Active Ion for Tunable Solid-State Lasers

P. 64

A. Seas, V. Petričević, and R. R. Alfano

FINAL REPORT

PRINCIPAL INVESTIGATOR: Prof. Robert R. Alfano

Period Covered: 11/01/91 - 10/31/93

Institute for Ultrafast Spectroscopy and Lasers
Physics Department, Room J-419
City College of New York
138 Street & Convent Avenue
New York, N.Y. 10031

GRANT NUMBER: NAG-1-1346

SUMMARY OF RESEARCH ACCOMPLISHMENTS

The following summarizes our major accomplishments made under the NASA grant: NAG-1-1346 "Tetravalent Chromium (Cr^{4+}) as Laser-Active Ion for Tunable Solid-State Lasers":

1. Numerical modeling of the four mirror astigmatically compensated, Z-fold cavity was performed. The simulation revealed several design parameters to be used for the construction of a femtosecond forsterite laser.

2. Generation of **femtosecond** pulses from a continuous-wave mode-locked chromium-doped forsterite (Cr^{4+}:Mg_2SiO_4) laser has been accomplished. The forsterite laser was actively mode-locked using an acousto-optic modulator operating at 78 MHz with two Brewster high-dispersion glass prisms for intra-cavity chirp compensation. Transform-limited sub-100-fs pulses were routinely generated in the TEM_{00} mode with 85 mW of continuous power (with 1% output coupler), tunable over 1230-1280 nm. The shortest pulses of 60-fs pulsewidth were measured.

3. Self-mode-locked operation of the Cr:forsterite laser was achieved. Synchronous pumping was used to mode locked the forsterite laser resulting in picosecond pulses, which in turn provided the starting mechanism for self-mode-locking. The pulses generated had a FWHM of 105 fs and were tunable between 1230 - 1270 nm.

4. Numerical calculations indicated that the pair of SF 14 prisms used in the cavity compensated for quadratic phase but introduced a large cubic phase term. Further calculations of other optical glasses indicated that a pair of SFN 64 prisms can introduce the same amount of quadratic phase as SF 14 prisms but introduce a smaller cubic phase. When the SF 14 prisms were replaced by SFN 64 prisms the pulsewidth was reduced to 50 fs. Great improvement was observed in the stability of the self mode-locked forsterite laser and in the ease of achieving mode-locking. Using the same experimental arrangement and a new forsterite crystal (Crystal 4) with improved FOM the pulse width was reduced to 36 fs.[1]

RESEARCH ACCOMPLISHMENTS

1. MODELING OF A FOUR-MIRROR ASTIGMATICALLY COMPENSATED CAVITY

The major disadvantage of the three mirror cavity used for mode-locking of the forsterite laser[2,3] is that when is used with long samples the beam area inside the gain medium is not uniform. This problem can be overcome by using a four mirror z-fold astigmatically compensated cavity. The z-fold astigmatically compensated cavity design takes advantage of symmetry to force the beam size in the xz and yz planes to be simultaneously minimum at the same spatial position in the laser medium[4].

The z-fold four mirror cavity design is shown in figure 1. The four mirror cavity can be thought of as a combination of two three mirror cavities as shown in figure 1. One three mirror cavity consists of mirrors R_1, R_2, and a flat mirror positioned at the image plane and the other consists of mirrors R_4, R_3 and the flat mirror at the image plane. Both cavities use half of the gain medium. The folding angles of the mirrors R_2 and R_3 that compensate for astigmatism can be estimated using eq.

$$2t\left(\frac{\left(n^2-1\right)\sqrt{n^2+1}}{n^4}\right)=2f\sin\theta\tan\theta \qquad (1)$$

where: t - Half the thickness of the gain medium

f - Focal length of the folding mirrors

n - Index of refraction of the gain medium

q - Angle of incidence of the folding mirrors

Numerical calculations were performed using eq. 1 to estimate the folding angle for mirrors R_2 and R_3 to achieve astigmatic compensation in the four mirror z-fold cavity. In the calculations it was assumed that $R_2 = R_3$. Figure 2 shows the folding angle as a function of the laser crystal thickness

in the case of the forsterite laser and assuming different values for the radius of curvature of the folding mirrors.

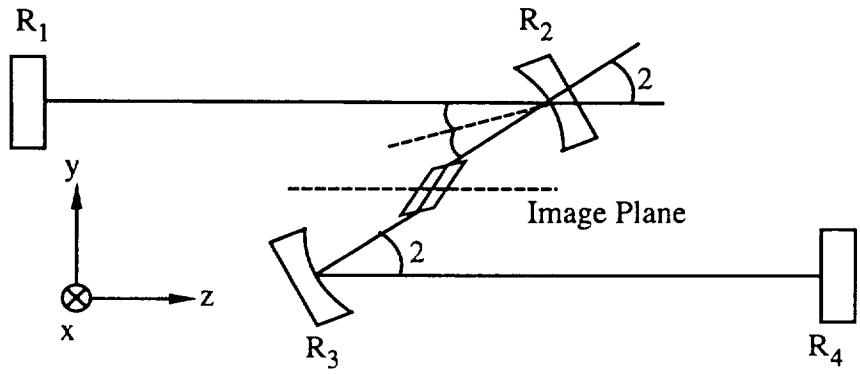

Fig. 1. Four mirror z-fold astigmatically compensated cavity design. θ is the folding angle of mirrors R_2 and R_3.

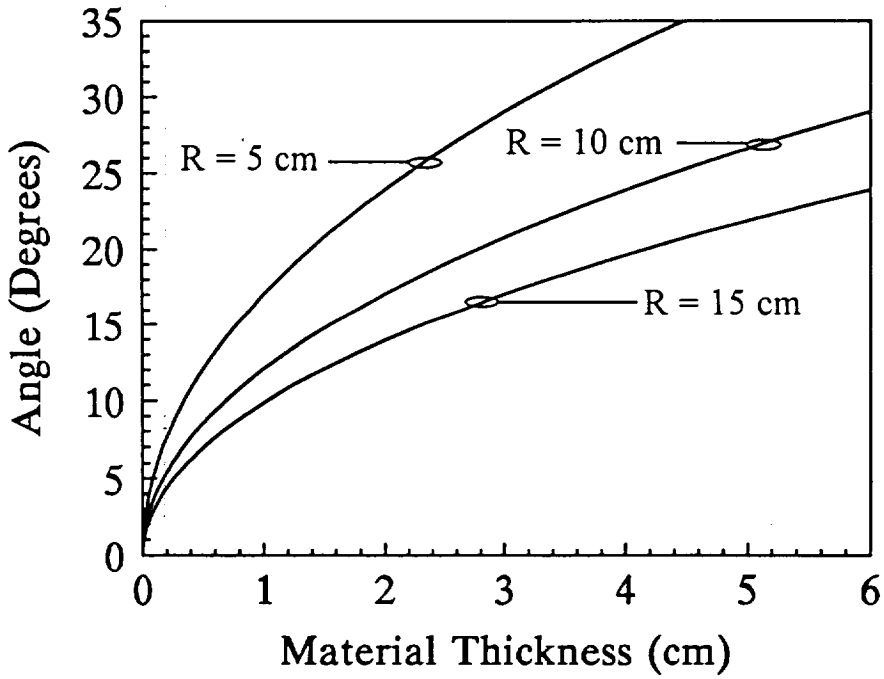

Fig. 2. Folding angle, θ, vs. forsterite crystal thickness for astigmatic compensation in a four mirror cavity.

Other characteristics of the four mirror cavity can be determined by using the theory presented in references 4 and 5. [5,6] A computer program was developed to simulate the beam size in the four mirror cavity used in the mode-locking experiments. For the program it was assumed that a 1 cm long chromium-doped forsterite crystal was positioned exactly at the center of the two folding mirrors R_2 and R_3. The round trip ABCD matrix of the four mirror cavity was calculated by choosing a reference plane and following the beam for a complete round trip through the cavity (see figure 3). Note that this process was performed twice, once for the xz and once for the yz plane since the folding mirrors and the brewster-cut crystal behave differently in the two planes

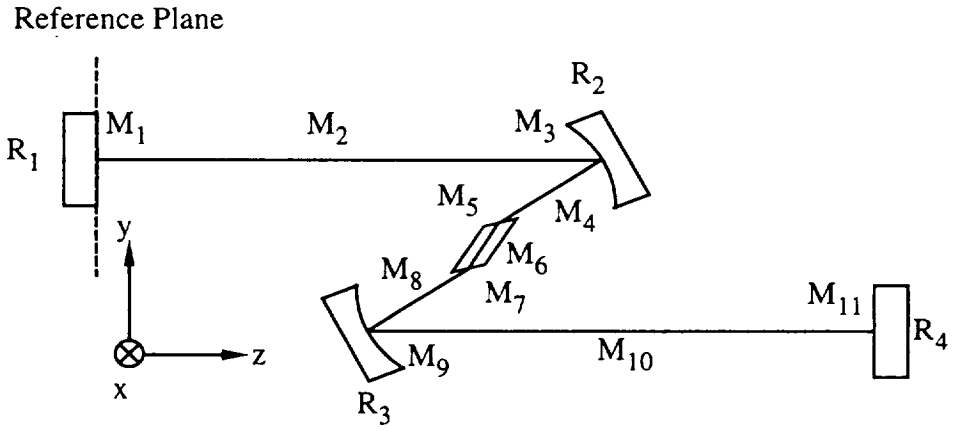

Fig. 3. Cavity configuration used in the numerical simulation.

The ABCD matrix for a complete round trip through the cavity is given by

$$M_t = M_2M_3M_4M_5M_6M_7M_8M_9M_{10}M_{11}M_{10}M_9M_8M_7M_6M_5M_4M_3M_2M_1$$

where: M_2, M_4, M_8, M_{10} - ABCD matrices for traveling a distance in free space

M_1, M_{11} - ABCD matrices for reflection from a flat mirror

M_9, M_3 - ABCD matrices for reflection from a curved mirror at an arbitrary angle of incidence (Different for the xz and yz planes)

M_5, M_7 - ABCD matrices for interface between air and forsterite crystal

M_6 - ABCD matrix for traveling in the forsterite crystal (Different for the xz and yz planes)

The stability range of the four mirror z-fold cavity design was determined next. This was done by determining the separation between mirrors R_2 and R_3 for which the self consistent and perturbation stable requirements were satisfied. The four mirror cavity is stable for ~± 1 mm from optimum separation between mirrors R_2 and R_3 which is similar to the three mirror cavity design .

When the stability range was determined, the distance between the folding mirrors was chosen around the center of the stability range and another program was written to calculate the size of the beam waist at any point inside the resonator. This was done by moving the reference plane through out the cavity and calculating the total ABCD matrix for the new reference plane. Then the beam waist at the reference plane was estimated using eq. 2.

$$\omega_2^2 = \frac{|B|\lambda}{\pi}\sqrt{\frac{1}{1-m^2}} \qquad (2)$$

where

$$m \equiv \frac{A+D}{2}$$

The results of the calculations are shown in figures 4 and 5. Figure 4 shows the size of the beam waist as a function of the position in the cavity while figure 5 is a magnified version of figure 4 showing the behavior of the beam inside the forsterite crystal. Considering figure 4 the beam waist at zero or at mirror R_1 has a value of about 600 μm and is the same for the xz and yz planes. This fact can serve as an indication when aligning the four mirror cavity. A nice round output beam

is indicative of astigmatic compensation while an elliptical beam at the output indicates that the folding angle is off the optimum value. The beam waist increases from 600 μm to 800 μm as it moves 85 cm from mirror R_1 to the folding mirror R_2. Still at mirror R_2 there is good agreement in the size in the xz and yz planes. Mirror R_2 has a radius of curvature of 10 cm, forcing the beam to focus 5 cm away from the mirror inside the forsterite crystal. As it can be seen from figure 5 the beams inside the forsterite laser have their minimum waist at exactly the same spot. Once the beam comes out of the forsterite crystal expands rapidly up to mirror R_3 which collimates the beam. Finally the beam moves from mirror R_3 to R_4 where it gets reflected and the same transformations are repeated.

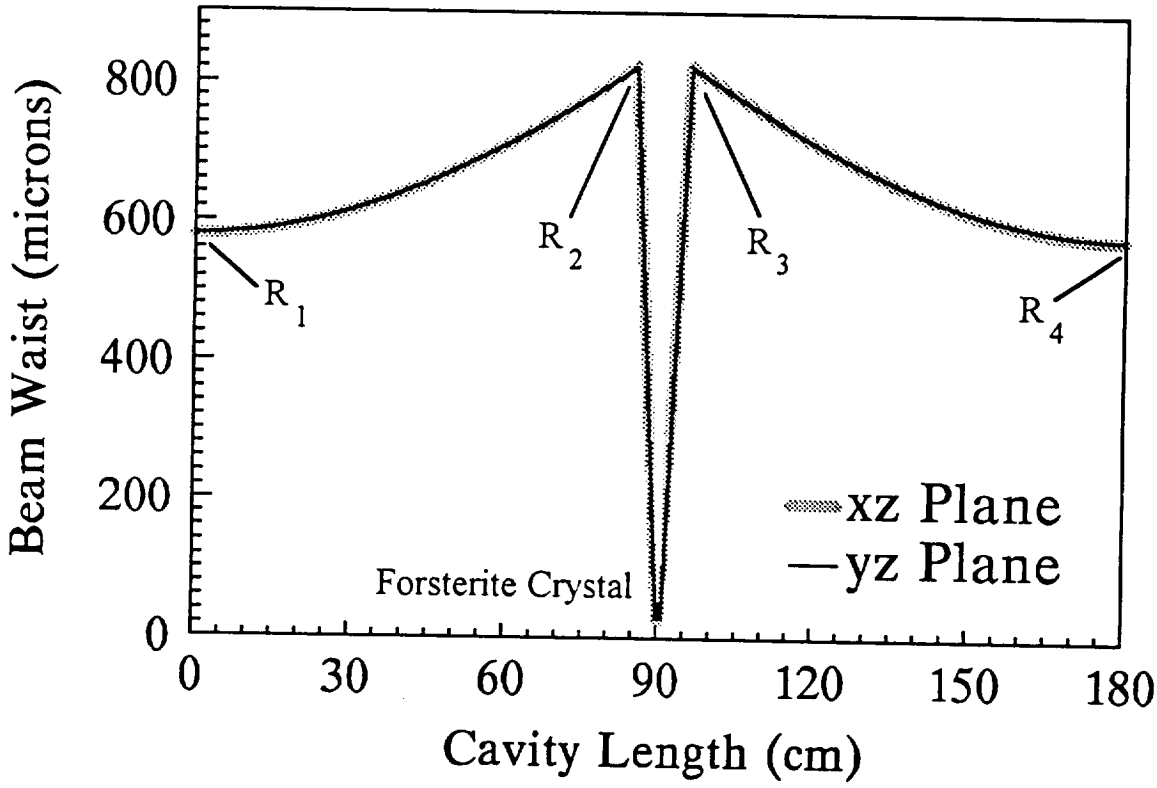

Fig. 4. Beam waist vs. position in the four mirror, z-fold, astigmatically cavity design.

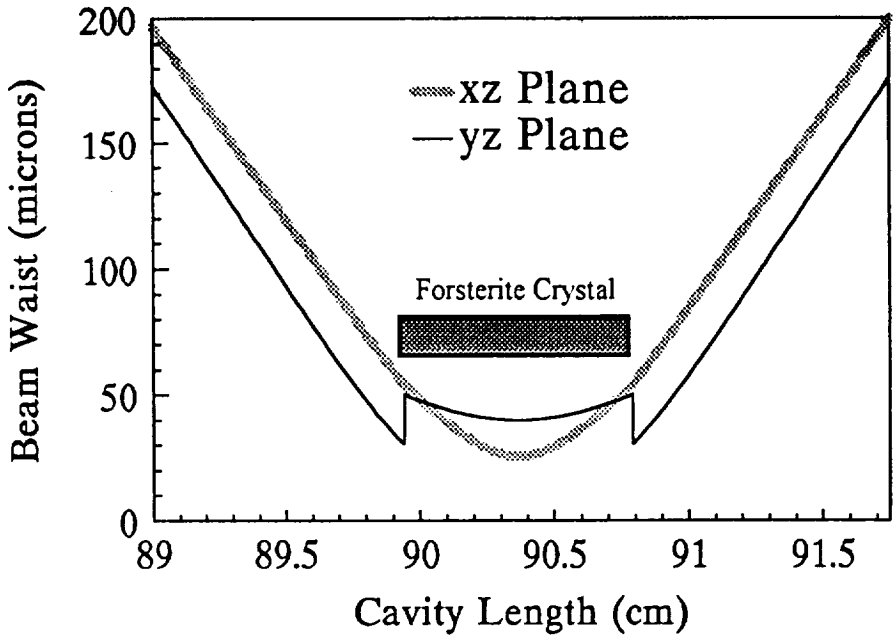

Fig. 5. Beam waist vs. position in the forsterite crystal for the four mirror, z-fold, astigmatically cavity design.

In order to be able to compare the results obtained from the analysis of the four mirror cavity design with the three mirror cavity the same computer program was modified to correspond to the three mirror cavity. For this program a 1 cm long brewster-cut forsterite crystal was placed in a three mirror cavity with R_1 = 5 cm, R = 10 cm, R_2 = flat and the same procedure as with the four mirror cavity was repeated. The results of this simulation are shown in figures 6 and 7. Figure 6 shows the size of the beam waist as a function of the position in the cavity while figure 7 is a magnified version of figure 6 showing the behavior of the beam inside the forsterite crystal.

By comparing figures 5 with 7 it is clear that a four mirror z-fold cavity design has better mode characteristics as compared to the three mirror cavity. The four mirror cavity compensates for the astigmatic effects introduced by the brewster forsterite crystal and also offers a uniform mode area in the forsterite crystal. The cavity mode can be easily matched with the pump mode. In the three mirror cavity design the minimum beam waists for the two planes are formed at different

positions in the forsterite crystal resulting in a non uniform mode area making hard to match pump and cavity modes. Sub-100-μm beam size is achieved using either cavity configuration.

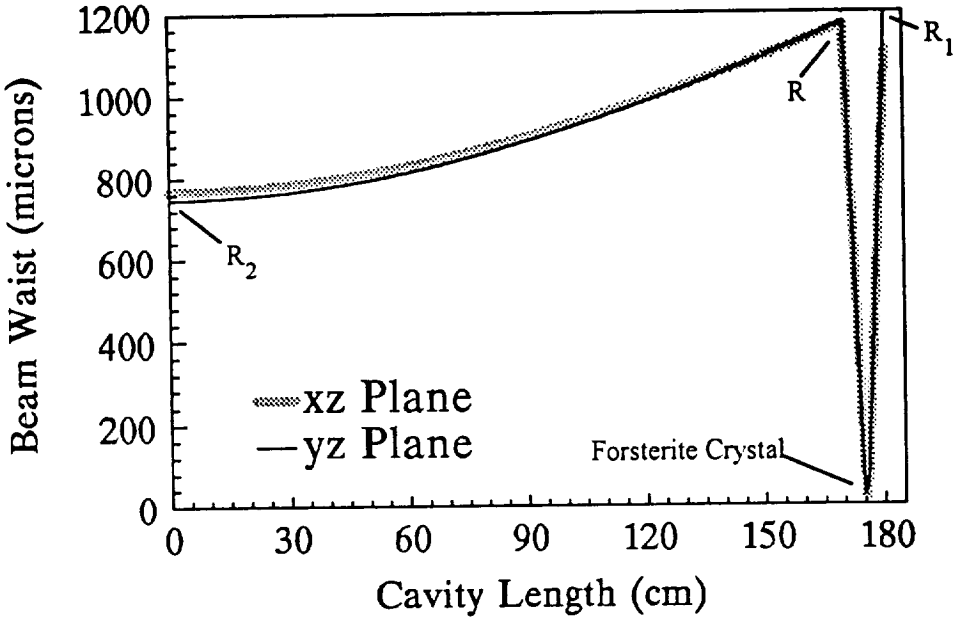

Fig. 6. Beam waist vs. position in the three mirror astigmatically compensated cavity design.

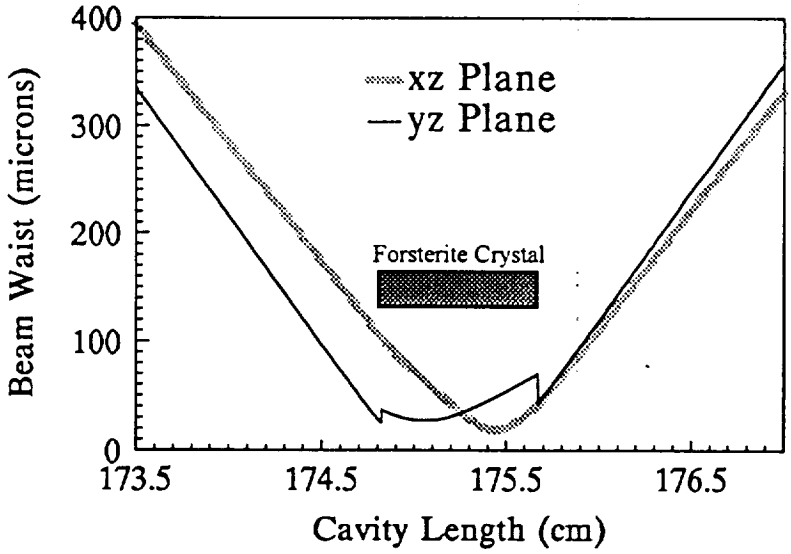

Fig. 7. Beam behavior inside the forsterite crystal in the three mirror astigmatically compensated cavity design.

2. CHROMIUM-DOPED FORSTERITE LASER GENERATES FEMTOSECOND PULSES

The generation of femtosecond pulses from a continuous-wave mode-locked chromium-doped forsterite (Cr^{4+}:Mg_2SiO_4) laser was accomplished. The forsterite laser was actively mode-locked using an acousto-optic modulator operating at 76 MHz with two Brewster high-dispersion glass prisms for intra-cavity chirp compensation. Transform-limited sub-100-fs pulses were routinely generated in the TEM_{00} mode tunable over 1230-1280 nm. The shortest pulses of 60-fs pulsewidth were measured and the for the first time the forsterite laser operated in the self-mode-locked mode.

The experimental arrangement is shown in Fig. 1. The Brewster-angle-cut forsterite crystal was placed in a four-mirror, z-fold astigmatically compensated cavity which is widely used for Ti:sapphire lasers. The combination of mirrors used was: a flat back mirror, two 10-cm-radius folding mirrors, and a flat output coupler. The transmission of the output coupler was 1% at the lasing wavelength, while the folding mirrors and the back mirror had reflectivity R=99.9% for the 1200-1300 nm range. The Cr:forsterite crystal used in this study was grown by the Mitsui Mining & Smelting Company, Japan . The length of the sample was 1 cm and the absorption coefficient at the pump wavelength of 1064 nm was $\alpha = 0.7224\ cm^{-1}$. To eliminate the need to chop the pump beam, the laser crystal was mounted in a copper block and was cooled by a single-stage thermoelectric cooler. Better thermal contact between the crystal and the copper block was achieved by wrapping the crystal in an indium foil. The crystal and the copper block were purged by nitrogen to prevent moisture condensation. The Cr:forsterite crystal was pumped by a continuous-wave Nd:YAG laser. The pump beam was focused by a 7.5-cm lens through the 10-cm-radius folding mirror into the crystal. The 1064-nm pump power incident on the forsterite crystal was 4.7 W. The output of the forsterite laser was monitored with a fast germanium detector and an oscilloscope, and the pulsewidth was measured with a real-time autocorrelator. The bandwidth of the mode-locked forsterite laser was measured using a lead sulfide (PbS) detector coupled to a 50-cm Jarrel Ash monochromator, equipped with 10-μm slits.

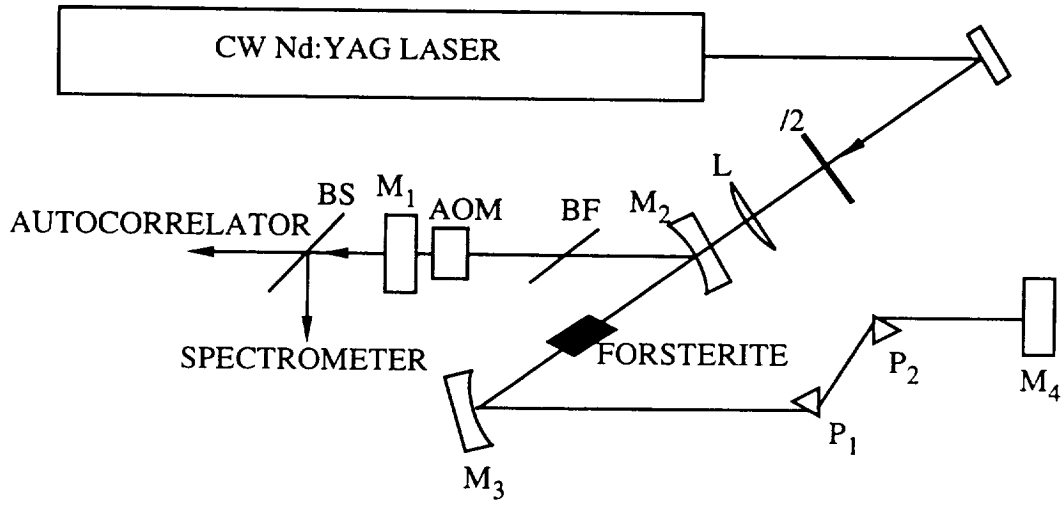

Fig. 1. Schematic diagram of the experimental arrangement for the actively mode-locked operation of the Cr:forsterite laser: $\lambda/2$, half-wave plate for 1064 nm; L, focusing lens; M_1, output mirror, M_2, M_3, 10-cm-radius folding mirrors; M_4, back mirror; AOM, acousto-optic modulator; BF, birefringent tuning plate; BS, beam splitter; P_1 and P_2, Schott SF 14 glass prisms.

Actively mode-locked operation of the forsterite laser was achieved when the acousto-optic modulator was inserted in the cavity. Mode-locking was observed when the length of the cavity was adjusted to a length of ~1.97 m corresponding to the frequency of the acousto-optic modulator (76 MHz). When the prisms are not part of the cavity a stable train of 6-ps pulses was obtained with a bandwidth-pulsewidth product of 1.34 indicating that the pulses were chirped.

To compensate for the dispersion, a pair of high-dispersion Schott SF 14 glass Brewster prisms were inserted in the cavity. A pair of prisms was expected to introduce negative group-velocity dispersion, without increasing the cavity loss. The distance between the prisms was varied until the shortest pulse width were measured, while maintaining the total length of the cavity constant.

The insertion of the pair of SF 14 prisms in the cavity resulted in a significant reduction of pulsewidth. We observed two distinct regimes where the forsterite laser would produce femtosecond pulses. In the first regime we had compensation of GVD introduced by the forsterite crystal. The shortest pulses measured in this case had duration of 900 fs FWHM and spectral width of 1.9 nm FWHM. Figure 2 (a) shows the autocorrelation trace of the pulsewidth and figure 2 (b) shows the corresponding spectrum for the 900 fs pulses. Circles represent experimental data and the solid line is the best fit $sech^2$ pulse shape was assumed for fitting. The pulsewidth-bandwidth product $\Delta\tau_p\Delta\nu = 0.33$, indicated nearly transform limited pulses.

Further optimization of the cavity (optimize the position of the forsterite crystal with respect to the two folding mirrors and the distance between the two folding mirrors) resulted in a significant reduction of pulsewidth, to less than 100 fs, with a spectral width of the order of 20 nm. An autocorrelation trace and the corresponding spectrum of a typical pulse are shown in figure 3 (a) and (b). The pulsewidth shown is 90 fs and the bandwidth is 19 nm. The pulsewidth-bandwidth product $\Delta\tau_p\Delta\nu = 0.32$, indicating transform-limited pulses for a $sech^2$ pulse. The optimum distance between the two prisms when stable 90-fs pulses were obtained, was determined to be 35 cm. Shorter pulses were observed after long hours of cavity optimization and only for brief times. The autocorrelation trace presented in figure 4 shows a pulse of less than 60 fs FWHM.

The reduction of the pulsewidth from 900 fs to 90 fs indicated that another mechanism besides active modulation is responsible for the shortening of the pulses. It was suspected that the self mode-locking mechanism was responsible for the generation of the 90 fs pulses. To investigate this possibility the RF power from the acousto-optic modulator was disconnected while stable sub-100-fs pulses were monitored. Within the first 30 seconds no change in the output was observed, i. e. stable sub-100-fs pulses were generated without any external modulation. The mode-locked operation usually ceased after this initial period, most likely due to some mechanical disturbances (Self mode-locking will be discussed in subsequent sections). This is an indication that the Cr:forsterite laser actually operated, similar to Ti:sapphire lasers in a self-mode locked

regime, where active mode-locking only sets the conditions necessary for self-mode-locked operation by producing intense optical fields in the cavity. Intensity-induced Kerr nonlinearities in the gain medium, combined with negative group velocity dispersion introduced by the prisms are responsible for production of the shortest pulses.

The actively mode-locked forsterite laser was tuned using an intracavity single-crystal quartz birefringent plate as shown in figure 1. With only one combination of laser mirrors the laser output was continuously tuned between 1230 - 1280 nm. The power output of 50 mW was measured, for 1.9 W of absorbed pump power. The pulsewidth and output power did not change significantly over the tuning range.

The dependence of the pulsewidth on the pump power was measured. As described above, when pumped by the maximum available power of 4.7 W incident on the crystal, stable sub-100-fs pulses were generated. As the pump power was lowered, the pulsewidth increased to above 1 ps at 3.9 W pump power incident on the forsterite crystal. The tendency of pulse shortening with increasing power suggests that, if more pump power were available, even shorter pulses may be obtained.

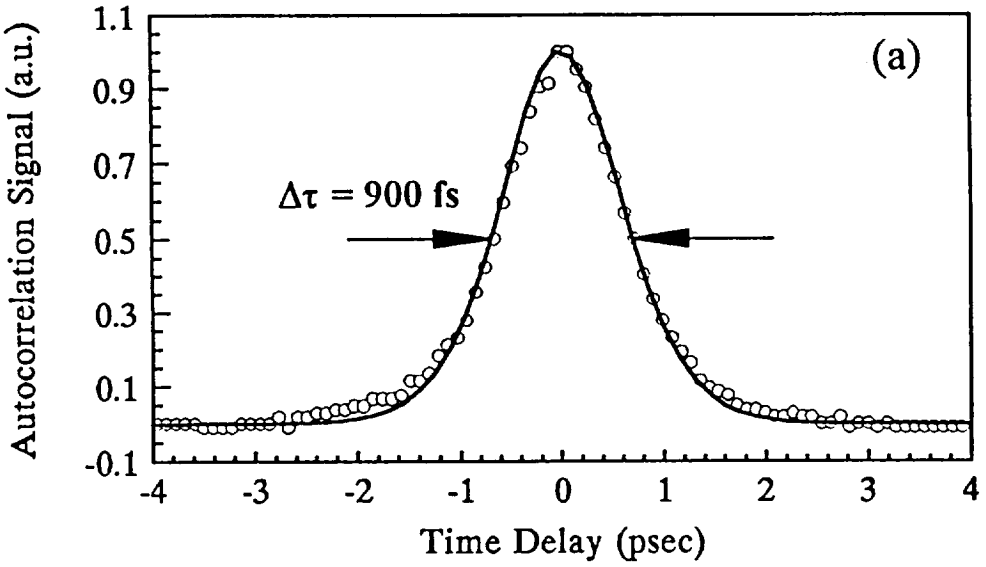

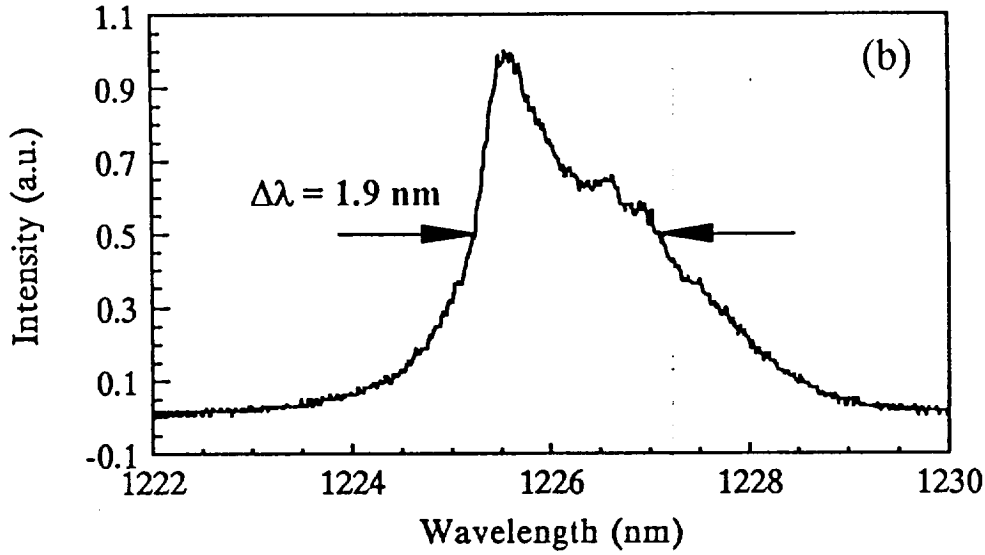

Fig. 2. An autocorrelation trace (a) and spectrum (b) of the 900 fs pulses. Circles represent experimental data and the solid line is the best fit. $sech^2$ pulse shape was assumed for fitting. The pulsewidth-bandwidth product is $\Delta\tau_p\Delta\nu = 0.33$.

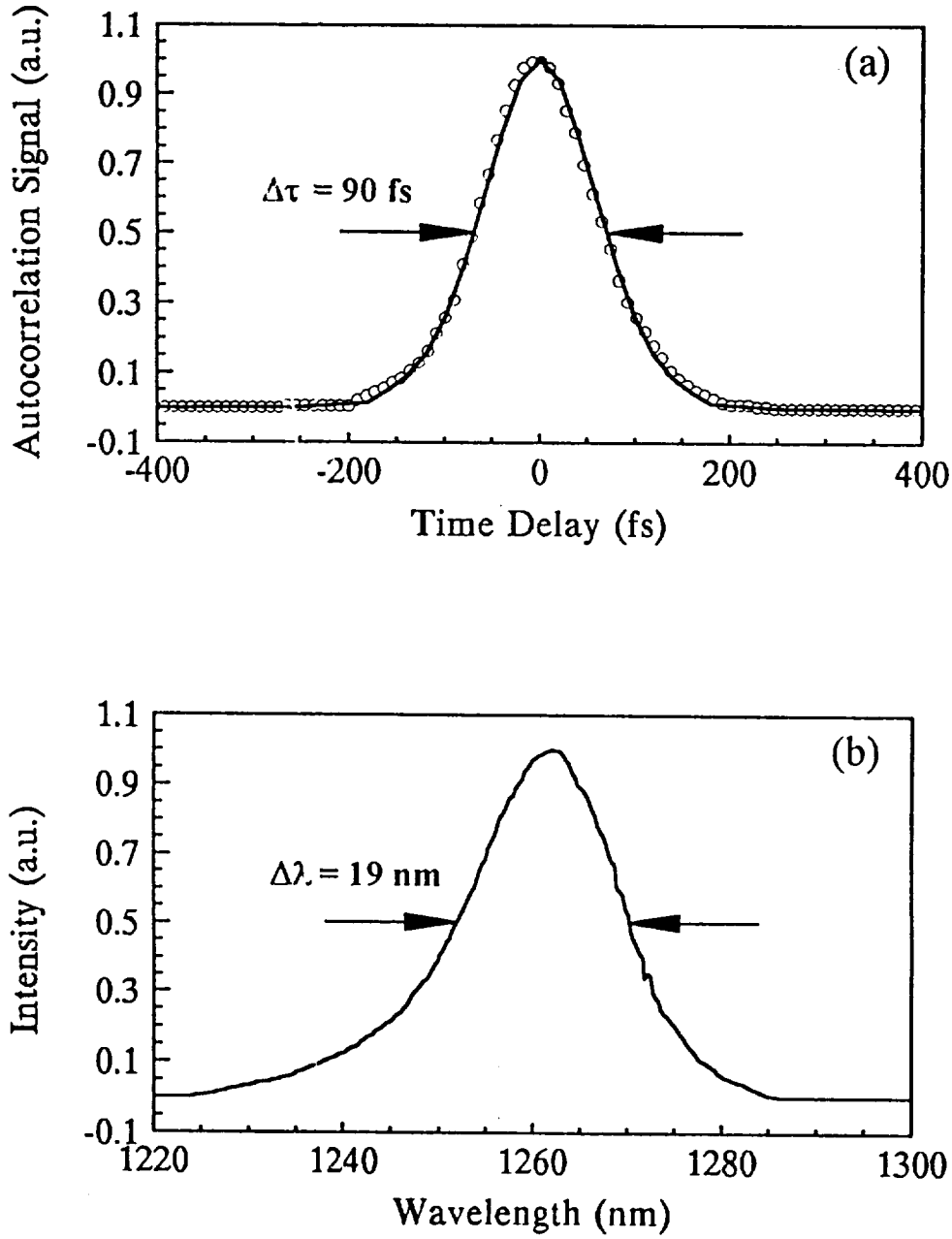

Fig. 3. An autocorrelation trace (a) and spectrum (b) of 90-fs pulses. Circles represent experimental data and the solid line is the best fit. $sech^2$ pulse shape was assumed for fitting. The pulsewidth-bandwidth product $\Delta\tau_p\Delta\nu = 0.32$.

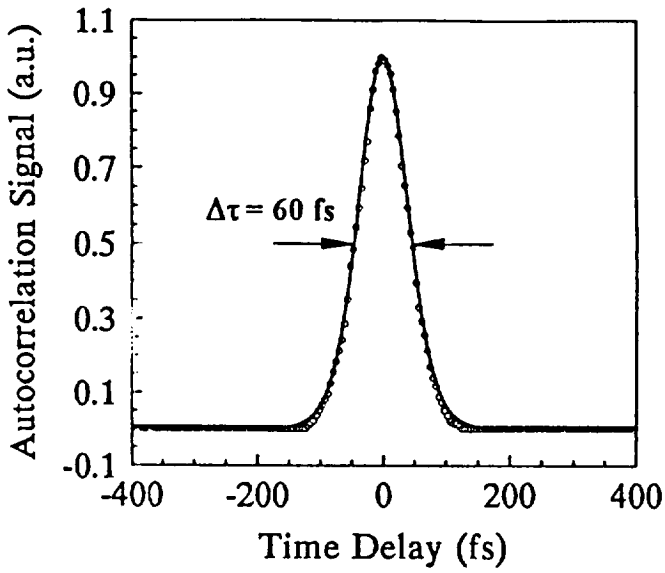

Fig. 4. An autocorrelation trace of 60-fs pulses (assuming $sech^2$ pulse shape). Circles represent experimental data and the solid line is the best fit.

3. SELF-MODE-LOCKED Cr:FORSTERITE LASER

The observed mechanism of generation of femtosecond pulses from the active-mode locked forsterite laser suggests that femtosecond pulses can be generated from chromium doped forsterite laser without the need of active modulation.[7] In order to achieve pure self mode locked operation we design the laser shown in figure 1. The cavity is the same four mirror astigmatically compensated cavity used before but now pumping is provided by a CW mode-locked Nd:YAG laser. We removed the acousto-optic modulator and the birefringent plate, and we inserted an aperture between the second prism and the end mirror M_4 for tuning purposes.

The main idea behind this experiment is that picosecond pulses will be generated by adjusting the length of the forsterite laser to match the frequency of the pumping CW mode-locked Nd:YAG laser (synchronously-pumped mode-locking). These picosecond pulses in turn will generate the passive modulation and provide the starting mechanism for self mode-locking.

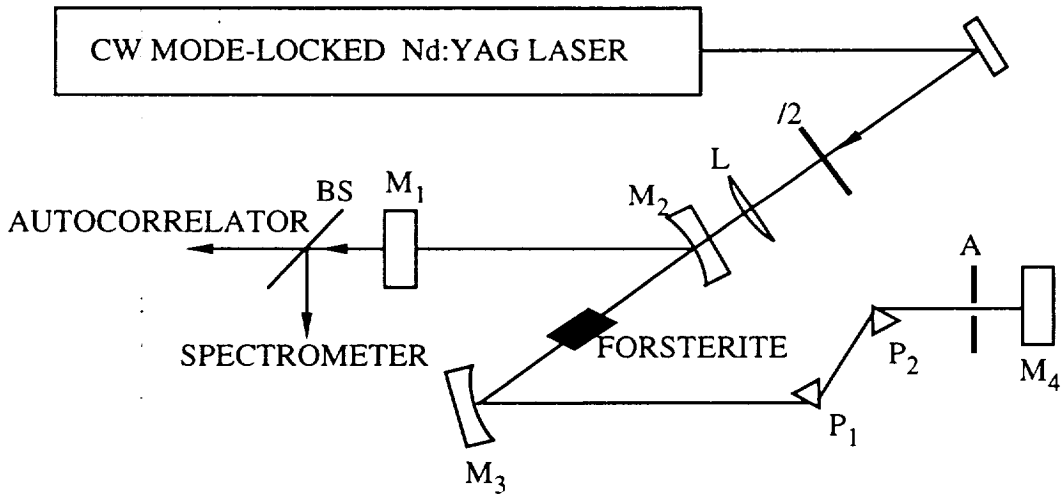

Fig. 1. Synchronously pumped forsterite laser design engineered for the generation of femtosecond pulses and self-mode-locking.

Synchronously pumped mode locking was observed when the length of the forsterite laser

cavity was matched to the length of the Nd:YAG laser. The output pulses of the synchronously pumped forsterite laser had duration of the order of 200-300 ps. By careful optimization of the cavity by adjusting the position of the laser crystal with respect to the two folding mirrors, the forsterite laser was self mode-locked and the pulsewidth was reduced to 105 fs with a spectral width of the order of 15 nm. In order to confirm that self mode-locking was achieved the cavity length was increased while monitoring the pulsewidth and the pulse train on the oscilloscope. The forsterite laser continued to generate femtosecond pulses even when the length of the cavity was changed by few centimeters. This clearly indicated that the forsterite laser was self mode-locked and that synchronously pumped mode-locking acted as the starting mechanism for self mode-locking. The output power of the forsterite laser when femtosecond pulses were generated was 60 mW.

An intensity autocorrelation trace and the corresponding spectrum of a typical pulse are shown in figure 2 (a) and (b). The pulsewidth shown is 105 fs and the bandwidth is 16 nm. The pulsewidth-bandwidth product $\Delta\tau_p\Delta\nu = 0.32$, indicating transform-limited pulses assuming $sech^2$ pulses.

Figure 3 shows an oscilloscope photograph of the interferometric autocorrelation trace of the output pulses. Since there is good visibility of the fringes at the wings of the pulse it is evident that the pair of prisms compensated for the chirp introduced by the forsterite crystal. The self mode-locked forsterite laser was tuned using an aperture mounted on a translation stage between prism P_2 and mirror M_4. Continuous tuning of the laser was achieved between 1240 and 1270 nm limited only by the dielectric coating of the mirrors. The duration of pulses did not vary throughout the whole tuning range.

The stability of the self mode-locked forsterite laser was greatly improved as compared with the previous experiments where the acousto-optic modulator was part of the cavity. The forsterite laser was operating in a self mode-locked mode for up to one hour without significant change in the output pulse characteristics. We believe that the improvement was mainly due to the absence of the losses and phase distortions due to the mode locker and the birefringent filter.

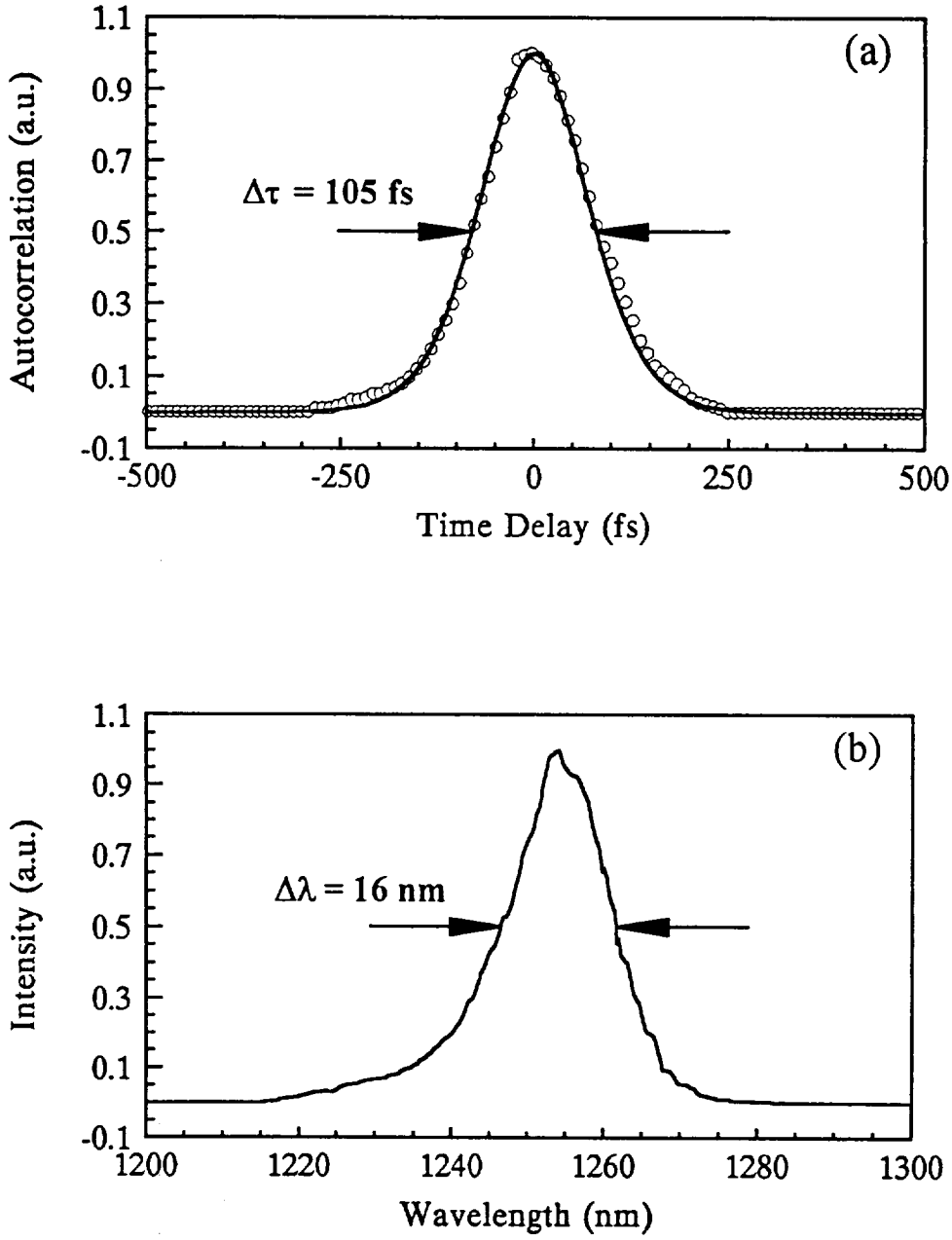

Fig. 2. An autocorrelation trace (a) and spectrum (b) of 105-fs pulses obtained from a z-fold cavity with SF 14 prisms for chirp compensation. Circles represent experimental data and the solid line is the best fit for $sech^2$ pulse shape.

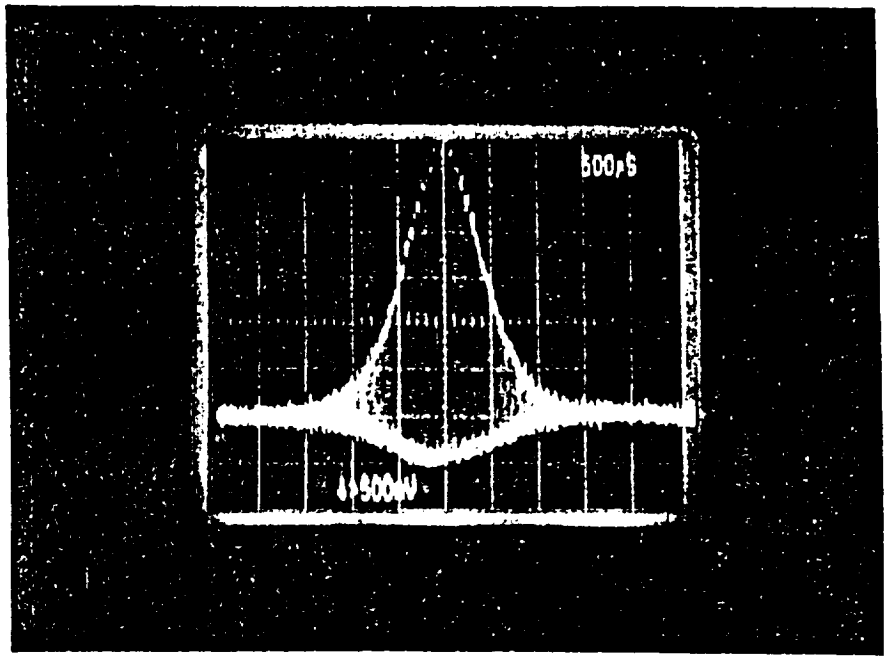

Fig. 3. Interferometric autocorrelation of the output pulses of the forsterite laser.

4. IMPROVED SELF-MODE-LOCKED OPERATION

4. 1. ELIMINATION OF CUBIC PHASE DISTORTIONS

The calculations and experimental results in the case of Cr:forsterite laser indicated that a pair of SF 14 prism can compensate for group velocity dispersion in the forsterite laser.[8] The optical characteristics of SF 14 optical glass for 1250 nm are n = 1.729, $dn/d\lambda = -0.02017\ \mu m^{-1}$, $d^2n/d\lambda^2 = 0.02262\ \mu m^{-2}$, and $d^3n/d\lambda^3 = -0.0999\ \mu m^{-3}$. The optimum distance between the two prisms was determined to be 35 cm when stable 105-fs pulses were obtained. Carrying out the calculation for the phase derivatives with respect to frequency we obtained $\partial^2\phi/\partial\omega^2 = -3273\ fsec^2$ and $\partial^3\phi/\partial\omega^3 = -2170\ fsec^3$ (for a round trip). This calculation indicates that SF 14 may not be the most appropriate glass for pulse shortening in this wavelength region since it introduces a large cubic phase term. Shorted pulses may be generated by using material which will introduce less cubic phase as is the case with Ti:sapphire.[9,10,11]

Calculations of higher order phase order terms introduced by a pair of prisms in the cavity were performed to determine optical glass that can compensate for GVD and introduce minimum cubic phase term. Table 1 lists the expressions used for the numerical evaluation of the dispersion characteristics of different optical materials.[12] Using these expressions the dispersion formula for the second and third order phase terms are evaluated and then the distance that these prism should be placed in order to introduce an equal amount of quadratic phase term as SF 14 prisms is determined. Then the amount of cubic phase by using the specific optical material is calculated.

Phase calculations were carried out for prism pairs for all the types of optical glasses listed in Schott catalogue. Table 2 lists the numerical results for some types of glass that can compensate for chirp in this wavelength region and introduce less cubic phase term. Column 1 lists the glass type. Columns 2 and 3 list the second and third derivative of the phase with respect to frequency for material dispersion, respectively and indicate the amount of quadratic and cubic phase that will be introduced to the pulse when it transverses length l_m of the specified material. Columns 4 and 5 list the second and third derivative of the phase with respect to frequency introduced by a pair of

prism with separation l_p, respectively. They indicate the amount of quadratic and cubic phase that will be introduced to the pulse when it passes through a pair of prism with separation l_p, assuming minimum glass pathway in the prisms. Column 6 shows the prism separation that will introduce the same quadratic phase term as SF 14 glass prisms, and the last column shows the cubic phase which will be introduced by using the specified type of glass for a prism separation which compensates for the quadratic phase. The values of phase derivatives shown for the pair of prisms are for round trip, l_p is measured in mm and the calculations were performed for λ=1250 nm.

Table 1. Second and third order derivatives of phase with respect to frequency for a double pair prism and material.

PRISM	MATERIAL
$\frac{d^2\Phi_p}{d\omega^2} = \frac{\lambda^3}{2\pi c^2}\frac{d^2P}{d\lambda^2}$	$\frac{d^2\Phi_m}{d\omega^2} = \frac{\lambda^3 l_m}{2\pi c^2}\frac{d^2n_m}{d\lambda^2}$
$\frac{d^3\Phi_p}{d\omega^3} = \frac{-\lambda^4}{4\pi^2 c^3}\left[3\frac{d^2P}{d\lambda^2} + \lambda\frac{d^3P}{d\lambda^3}\right]$	$\frac{d^3\Phi_m}{d\omega^3} = \frac{-\lambda^4}{4\pi^2 c^3}\left[3\frac{d^2n_m}{d\lambda^2} + \lambda\frac{d^3n_m}{d\lambda^3}\right]$

Where

$$\frac{d^2P}{d\lambda^2} = 4\left[\frac{d^2n}{d\lambda^2} + \left(2n + \frac{1}{n^3}\right)\left(\frac{dn}{d\lambda}\right)^2\right] l_p \sin\beta - 8\left(\frac{dn}{d\lambda}\right)^2 l_p \cos\beta$$

and

$$\frac{d^3P}{d\lambda^3} = 4\frac{d^3n}{d\lambda^3} l_p \sin\beta - 24\frac{dn}{d\lambda}\frac{d^2n}{d\lambda^2} l_p \cos\beta$$

Table 2 Dispersion characteristics for different optical glasses at 1250 nm

1	2	3	4	5	6	7
Glass Type	$\frac{d^2\Phi_m}{d\omega^2}$ (fsec^2)	$\frac{d^3\Phi_m}{d\omega^3}$ (fsec^3)	$\frac{d^2\Phi_p}{d\omega^2}$ (fsec^2)	$\frac{d^3\Phi_p}{d\omega^3}$ (fsec^3)	l_p (mm)	$\frac{d^3\Phi_p}{d\omega^3}$ (fsec^3)
SF 14	78 l_m	130 l_m	662 - 11.2 l_p	974 - 9.0 l_p	350	-2170
SF 15	63 l_m	110 l_m	532 - 8.5 l_p	827 - 5.2 l_p	451	-1504
SF 2	52 l_m	93 l_m	436 - 56.5 l_p	706 - 3 l_p	573	-1008
SFN 64	61 l_m	115 l_m	516 - 9.9 l_p	859 - 3.2 l_p	384	-359
F 2	45 l_m	87 l_m	376 - 5.8 l_p	662 - 1.4 l_p	629	-214
BaSF 1	43 l_m	81 l_m	361 - 5.2 l_p	621 - 1.5 l_p	698	-394
LaF 13	54 l_m	107 l_m	461 - 9 l_p	794 - 1.5 l_p	417	+171
LaFN 7	53 l_m	115 l_m	460 - 10.3 l_p	853 - 0.02 l_p	364	+848

Figure 1 shows the cubic phase for different types of prisms vs. wavelength assuming that the prism separation is set to compensate for the quadratic phase in the forsterite laser cavity, and minimum glass pathway in the prisms. As is indicated SF 14 prisms introduce a large cubic phase at 1250 nm but will be more appropriate to be used for chirp compensation when the forsterite laser operates beyond 1300 nm. In figure 1 we also show other types of prisms that can be used for chirp compensation in the tuning range of chromium doped forsterite.

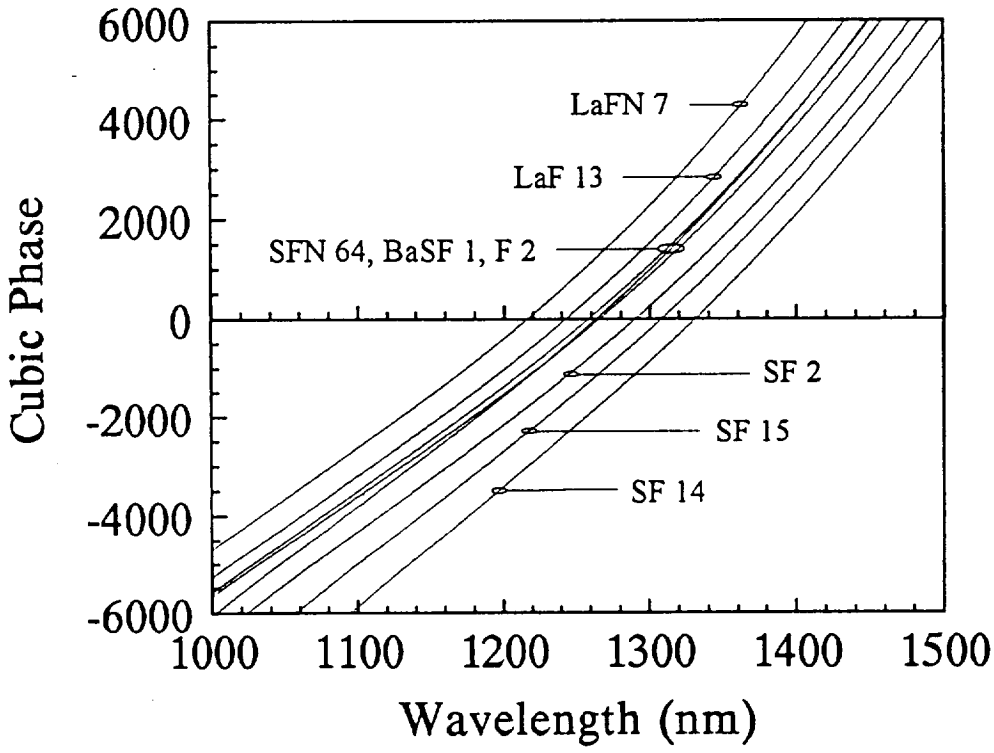

Fig. 1. Round-trip cubic phase of various Brewster prism pairs. Zero round-trip cavity quadratic phase and minimum glass pathway in the prism are assumed.

4. 1 GENERATION OF 36-fs PULSES BY A SELF-MODE-LOCKED Cr:FORSTERITE LASER

The results of the calculations shown in table 2 and in figure 1 suggest that for 1250 nm other types of glass can compensate for group velocity dispersion and will introduce a smaller cubic phase term as compared with SF 14 prisms. We chose to use prisms made of SFN 64 glass because the prism separation was very close to the one for SF 14 prisms and our cavity design would required minimum changes.

The experimental arrangement used for the following experiments is exactly the same as the one described elsewhere[2] except that the SF 14 prisms were replaced with SFN 64 prisms. As before synchronously pumped mode locking was observed when the length of the forsterite laser cavity was matched to the length of the Nd:YAG laser, generating pulses with FWHM of 200-300 ps. By further optimization of the laser cavity the forsterite laser was self mode-locked generating sub-100-fs pulses. The stability of the self mode-locked forsterite laser and the ease of starting self mode-locking was improved as compared when SF 14 prisms were used. The prism separation for optimum operation was measured to be ~42 cm which is good agreement with 38.4 cm calculated. An intensity autocorrelation trace and the corresponding spectrum of a typical pulse are shown in Fig. 2 (a) and (b). The pulsewidth shown is 50 fs and the bandwidth is 33 nm. The pulsewidth-bandwidth product $\Delta\tau_p\Delta\nu = 0.32$ indicates transform-limited $sech^2$ pulses.

Further improvement in the pulsewidth of the output pulses from the self-mode-locked forsterite laser was achieved when the forsterite crystal was replaced with a new forsterite crystal. The new forsterite crystal had a Figure of Merit of 58 which is the highest FOM measured for any crystals tested so far. An intensity autocorrelation trace and the corresponding spectrum of a typical pulse are shown in Fig. 3 (a) and (b). The pulsewidth shown is 36 fs and the bandwidth is 52.5 nm. The pulsewidth-bandwidth product $\Delta\tau_p\Delta\nu = 0.368$ indicating nearly transform-limited $sech^2$ pulses. The pulses are not totally transform-limited probably due to phase distortions introduced by the 0.5 inch thick output coupler and the 300 μm thick beam splitter in the autocorrelator.

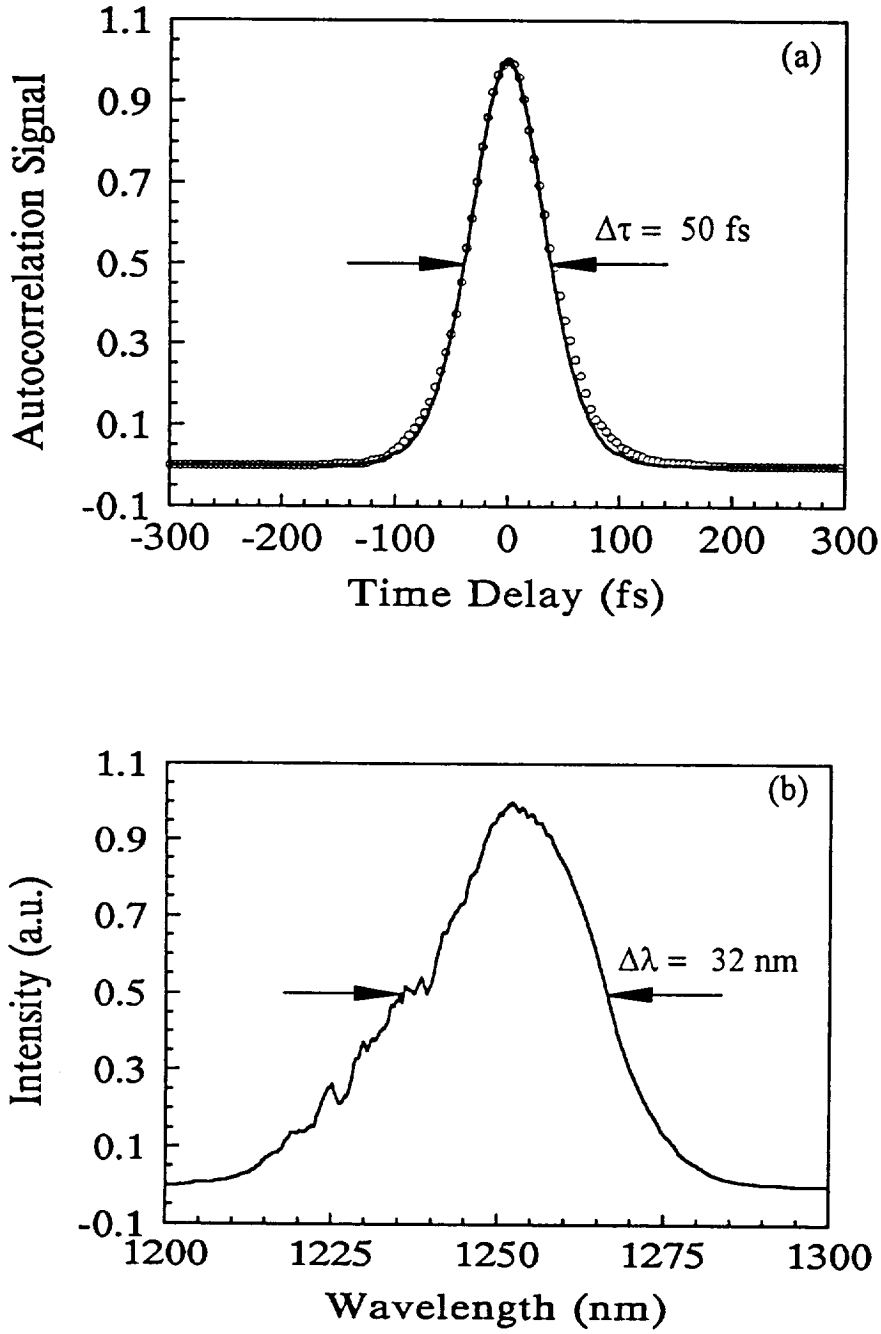

Fig. 2. An autocorrelation trace (a) and spectrum (b) of 50-fs pulses obtained from a z-cavity with SFN 64 prisms for chirp compensation. Circles represent experimental data and the solid line is the best fit for $sech^2$ pulse shape.

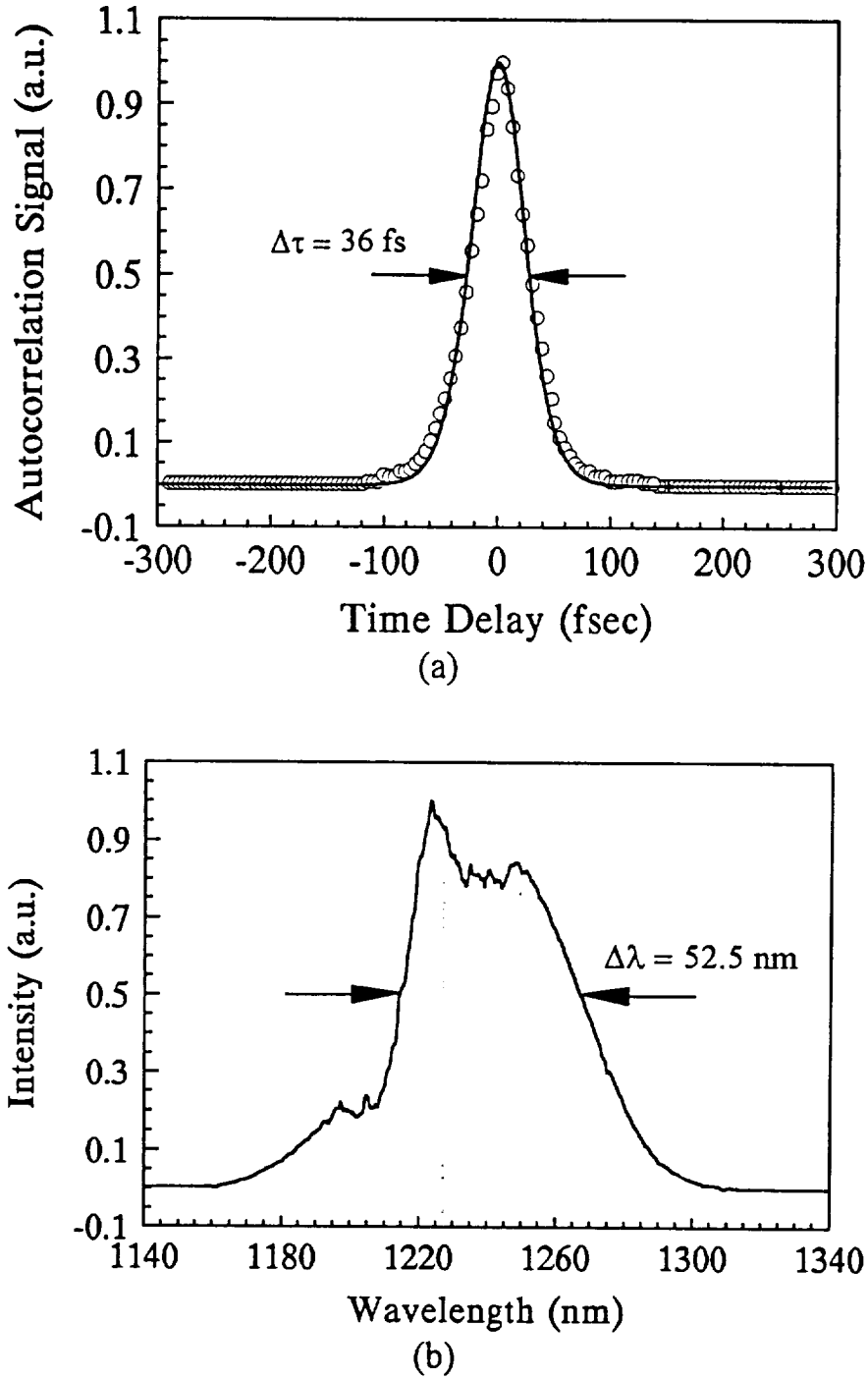

Fig. 3. An autocorrelation trace (a) and spectrum (b) of 36-fs pulses obtained from a z-fold cavity with SFN 64 prisms for chirp compensation. Circles represent experimental data and the solid line is the best fit for $sech^2$ pulse shape.

The stability of the self-mode-locked Cr:forsterite laser was improved when the new crystal was used in the cavity. The laser was operating in a self mode-locked mode of operation for as long as required without degradation in the quality of the output pulses. As seen from the bandwidth measurements the corresponding spectrum of the 36-fs pulses nearly covers the whole emission spectrum of forsterite (1170 - 1310 nm).

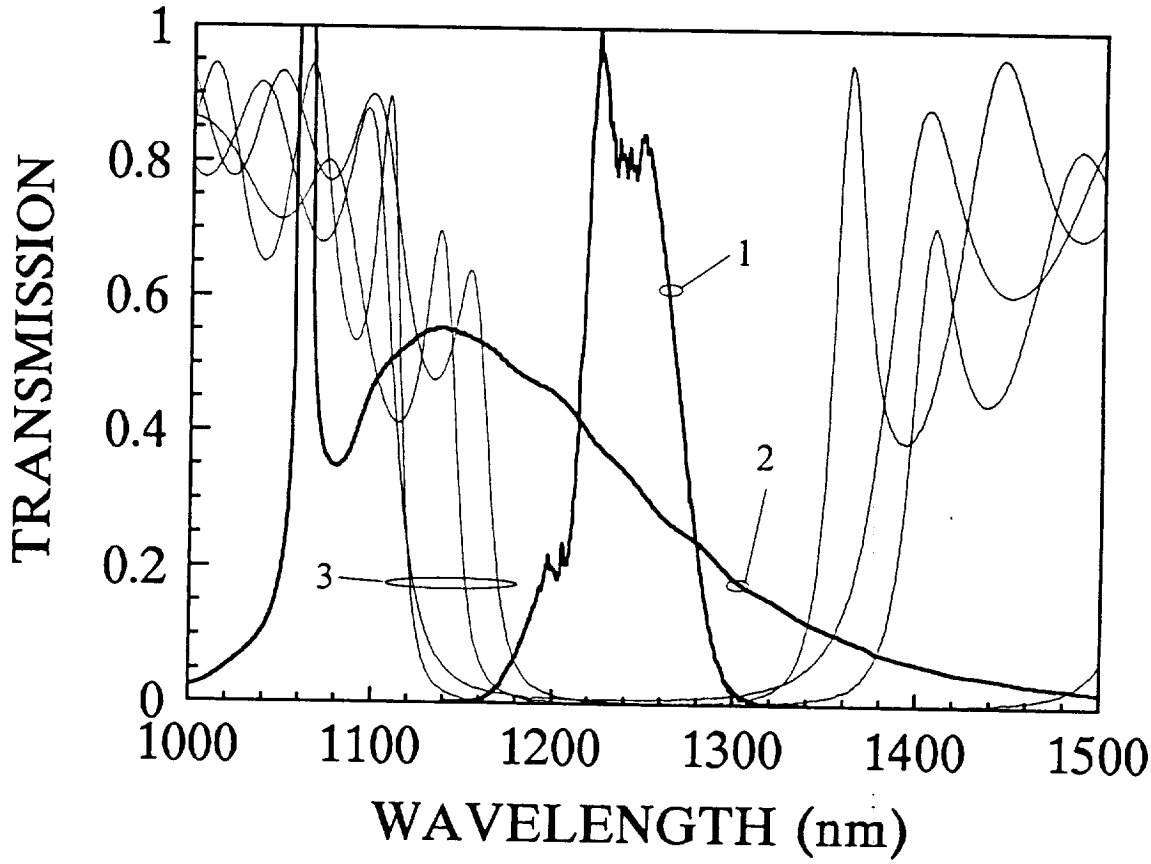

Fig. 5.7.3. Transmission of the mirror coatings forming the four mirror cavity, emission spectrum of Cr:forsterite when excited with 1064 nm radiation, and corresponding spectrum of the 36-fs pulses.

The 36-fs pulses generated by the self-mode-locked forsterite laser are longer that the pulses that will be generated if all of the emission spectrum is used. Figure 5.7.3 the dielectric

coatings of the mirrors used, the emission spectrum of the forsterite crystal and the corresponding bandwidth of the 36-fs pulses are plotted using the same axis. The bandwidth of the 36-fs pulses correspond to all the spectrum that the dielectric coatings would support. Mirrors with appropriate coatings will definitely generated shorter pulses where the whole emission spectrum of the Cr:forsterite laser is used.

PAPERS AND ABSTRACTS PUBLISHED DURING THE GRANT PERIOD (Copies are attached)

1. A. Seas, V. Petričević, and R. R. Alfano, "Generation of Sub-100-fs Pulses From a Continuous-Wave Mode-Locked Chromium-Doped Forsterite Laser", postdeadline paper presented at the Conference on Lasers and Electro-Optics (CLEO), Anaheim, California, May 11-15, 1992.

2. A. Seas, V. Petričević, and R. R. Alfano, "Generation of Sub-100-fs Pulses From a Continuous-Wave Mode-Locked Chromium-Doped Forsterite Laser", Opt. Lett. **17**, 937 (1992).

3. V. Petričević, A. Seas, and R. R. Alfano, "Novel Cr^{4+}-Based Tunable Solid-State Lasers", *Recent Advances in the Uses Of Light in Physics, Chemistry, Engineering and Medicine*, Daniel L. Akins and Robert R. Alfano, Editors, Proc. SPIE 1599, pp. 209-215 (1992).

4. A. Seas, V. Petričević, and R. R. Alfano, "60-fs Chromium-Doped Forsterite (Cr^{4+}:Mg_2SiO_4) Laser ", postdeadline paper presented at the International Conference Ultrafast Phenomena VII, Antibes-Juan les Pins, France, June 8-12, 1992.

5. A. Seas, V. Petricevi ć, and R. R. Alfano, "CW Mode-Locked Chromium-Doped Forsterite Laser Generates Tunable Sub-100-fs Pulses", presented at the 1992 Annual Meeting of the Optical Society of America , Albuquerque, New Mexico, September 20-25, 1992.

6. A. Seas, V. Petričević, and R. R. Alfano, "Generation of Ultrashort Pulses From Cr^{4+}:Forsterite", presented at the IEEE/LEOS 1992 Annual Meeting, Boston, Massachusetts, November 16-19, 1992.

7. V. Petričević, A. Seas, and R. R. Alfano, "Current Advances in the Development of Femtosecond Forsterite Lasers", presented at the SPIE's International Simposia on Optelectronic Packaging and Interconnects, Laser Engineering, and Biomedical Optics, Los Angeles, California, 16-23 January 1993.

8. A. Seas, V. Petričević, and R. R. Alfano, "Femtosecond Pulses Generated From a Synchronously Pumped Chromium-Doped Forsterite Laser", presented at the Topical Meeting on Advanced Solid-State Lasers, New Orleans, Louisiana, February 1-3, 1992.

9. V. Petričević, A. Seas, and R. R. Alfano, "Current advances in the development of femtosecond forsterite lasers", to be published in the Proceedings of SPIE's International Simposia on Optelectronic Packaging and Interconnects, Laser Engineering, and Biomedical Optics, Los Angeles, California, January 16-23, 1993

10. V. Petričević, A. Seas, and R. R. Alfano, "Cr:Mg_2GeO_4 and Cr:$CaMgSiO_4$: New Potential Tunable Solid-State Laser Crystals", To be published in the Proceedings at the Topical Meeting on Advanced Solid-State Lasers, New Orleans, Louisiana, February 1-3, 1992.

11. A. Seas, V. Petričević, and R. R. Alfano, "Self Mode-Locked Chromium-Doped Forsterite Laser Generates 50-fs Pulses", Opt. Lett. **18**, 891 (1993).

12. A. Seas, V. Petricevi ć, and R. R. Alfano, "Self Mode-Locked Forsterite Laser", presented at the Conference on Lasers and Electro-Optics (CLEO), Baltimore, Maryland, May 4-6, 1993.

13. A. Seas, "Generation of Ultrashort Pulses from Chromium Doped Forsterite Laser", Ph. D. Thesis, Graduate School of the City University of New York, July 1993.